EESTI MAAÜLIKOOL
Metsanduse ja inseneeria instituut

Julija Helm-Katšalov

SnO_2 NANOMATERIALS FOR LITHIUM-ION BATTERY APPLICATIONS

SnO_2 NANOMATERJALIDE KASUTUS LIITIUMIOONAKUDES

Bachelor's thesis
Engineering

Supervisors: Prof. Protima Rauwel, *PhD*
Prof. Erwan Yann Rauwel, *PhD, DSc*
Mr. Reynald Songphon Ponte, *MSc*

Tartu 2023

www.emu.ee
Eesti Maaülikool
Estonian University of Life Sciences

Eesti Maaülikool Kreutzwaldi 1, Tartu 51006		Bakalaureusetöö lühikokkuvõte	
Autor: Julija Helm-Katšalov		Õppekava: Tehnika ja tehnoloogia (384)	
Pealkiri: SnO_2 nanomaterjalide kasutus liitiumioonakudes			
Lehekülgi: 43	Jooniseid: 18	Tabeleid: 4	Lisasid: 1

Osakond / Õppetool: Energiakasutuse õppetool

ETIS-e teadusvaldkond ja CERC S-i kood: 4. Loodusteadused ja tehnika

4.17 Energeetikaalased uuringud; T140 Energeetika; T150 Materjalitehnoloogia

Juhendaja(d): Prof. Protima Rauwel, PhD; Prof. Erwan Yann Rauwel , DSc, PhD;

Mr. Reynald Ponte, MSc

Kaitsmiskoht ja -aasta: Tartu, 2023

Liitiumioonakud on Euroopa Liidu energiasüsteemi ümberkujundamisel üliolulised, kuid nende praegune energiamahutavus on ebapiisav, seetõttu on vaja leida uusi lahendusi. Üheks võimaluseks on kasutada tina oksiidi (SnO_2) nanomaterjale, mis on pooljuhid ja tsooniteooria kohaselt on nende keelutsooni energia 3.6 eVi (elektronvolt). See võimaldab parandada liitiumioonakude elektrokeemilisi omadusi, pikendades nende eluiga ja suurendades energiamahutavust. Oluline on leida õiged SnO_2 sünteesimistingimused, mis on seotud elektrooniliste omadustega, sealhulgas keelutsooni energiaga.

Käesoleva bakalaureusetöö peamine eesmärk on UV-spektroskoopia abil määrata viie erineva SnO_2 nanomaterjali keelutsooni energia ja uurida seeläbi temperatuuri ja sünteesiaja mõju nende elektroonilistele omadustele. UV spektri tulemuste põhjal analüüsiti Tauc arvutusmeetodil saadud tulemusi, kus ei avaldu otsese keelutsooni olulisi erinevusi, kuid kaudne keelutsoon näitab varieerumisi, mis võib olla tingitud nanomaterjalide erinevast suurusest, kujust, faasist või koostisest. Uurides SnO_2 defektiseisundeid nähtavas neeldumisspektris sünteesiaja suurenedes näitab, et pikema sünteesiajaga tekib materjalis rohkem defektitasandeid. Selleks, et mõista ja selgitada välja, mis põhjustab seesuguseid keelutsooni muutusi ja materjali defekte, tuleks teostada edasisi uuringuid. Tulevikus tehtav elektrokeemiline analüüs võib võimaldada korrelatsiooni elektrooniliste- ja elektrokeemiliste omaduste ning sünteesitingimuste vahel, võimaldades seeläbi toota optimaalseid nanomaterjale, mida saame kasutada liitiumioonakude edasiseks arendamiseks.

Märksõnad: SnO_2, nanomaterjalid, UV-spektroskoopia, Tauc graafikud, keelutsoon

www.emu.ee
Eesti Maaülikool
Estonian University of Life Sciences

Estonian University of Life Sciences Kreutzwaldi 1, Tartu 51006		Abstract of Bachelor's Thesis	
Author: Julija Helm-Katšalov		Curriculum: Engineering (384)	
Title: SnO_2 Nanomaterials for Lithium-Ion Battery Applications			
Pages: 43	Figures: 18	Tables: 4	Appendixes: 1

Department / Chair: Chair of Energy Application Engineering

Field of research and (CERC S) code: 4. Natural Sciences and Engineering

4.17 Energetic Research; T140 Energy Research; T150 Material Technology

Supervisors: Prof. Protima Rauwel, PhD; Prof. Erwan Yann Rauwel, DSc, PhD;

Mr. Reynald Ponte, MSc

Place and date: Tartu, 2023

Lithium-ion batteries are critical for the EU's energy transition, but their current energy capacity is insufficient. Tin oxide (SnO_2) nanomaterials, as a semiconductor with a bandgap of 3.6 eV (electron volt), can improve the electrochemical properties of Li-ion batteries, by increasing their lifespan and resolving low energy capacity issues. Electronic properties such as bandgap are linked to synthesis conditions.

The main goal of this bachelor's thesis is to determine the bandgap of five different samples of SnO_2 nanomaterials using UV-visible spectroscopy to investigate the effect of temperature and synthesis time on their electronic properties. Using a Tauc plot of the UV-visible spectra, bandgaps are determined. Temperature and synthesis time show a variation in the indirect bandgap but no significant impact on the direct bandgap. Defect states of SnO_2 can be seen in the visible absorption spectra. As the synthesis time increases, more defects are created in the material. This might be caused by different nanomaterial sizes, shapes, phases, or compositions; however, due to the lack of information, no conclusion can be drawn. Further investigation is needed to understand these bandgap variations. The future electrochemical analysis will make it possible to correlate the synthesis conditions with electronic and electrochemical properties, resulting in the best nanomaterials for battery applications.

Keywords: SnO_2, nanomaterials, UV-Vis spectroscopy, Tauc plot, bandgap

TABLE OF CONTENTS

INTRODUCTION

Batteries play a significant role in our daily lives, serving as a critical component in numerous technologies and systems that society relies on. With the widespread use of portable devices such as smartphones, laptops, and wearable devices, the demand for small and lightweight batteries has become omnipresent and indispensable. Furthermore, they are used as backup power sources in uninterruptible power supply systems, ensuring the continuous operation of vital systems like computer networks and medical equipment during power outages or brownouts.[1]

In light of the global mission to reduce carbon emissions, batteries are essential for promoting the transition to a climate-neutral economy. They facilitate this transition by enabling the production of more sustainable electric vehicles (EVs) and supporting the widespread development of renewable energy sources. Batteries serve as efficient energy storage systems that optimise the long-term functioning of a novel grid [2].

Among the various types of batteries available, lithium-ion batteries (LiBs) offer several key advantages. Notably, their high energy density allows for the storage of significant energy in a compact and lightweight package. This makes them ideal for use in portable electronic devices like smartphones, laptops, and tablets, as well as in EVs, where considerations of weight and space are crucial. Their high energy density, long cycle life, efficiency, and fast charging capabilities contribute to their attractiveness as a rapidly growing industry.

Multiple types of LiBs exist and each with its unique chemistry and respective performance characteristics. The most common and commercialized lithium-ion batteries are made of graphite anode material. However, their limited capacity and short lifespan pose significant challenges for researchers, particularly for EV applications. The short lifespan of LiBs mainly stems from the formation of a solid electrolyte interface on the anode's surface, leading to energy capacity loss and electrode degradation. Metal oxides (*e.g.*, TiO_2, CoO, SiO_2, SnO_2, *etc*.) added to the graphite anode can lead to longer duration and enhance energy density of the battery but do not solve the cycle life issue as they lead to coarsening of metal oxides materials, followed by electrode pulverization. Nevertheless, numerous studies have shown that these metal oxides tailored as nanoscale materials can significantly increase

anode performances. Therefore, the use of nanostructured materials presents a viable solution for meeting the demand for energy storage technology, as it improves battery performance while reducing costs. This makes batteries more practical and affordable for a broader range of applications. [3]

SnO_2 nanoparticles have aroused a keen interest among scholars due to their remarkable environmental and physical and chemical properties, *i.e.*, lightness, stability, and cost-effectiveness [4]. Sn-based materials, particularly SnO_2, are being extensively studied for their potential applications in LiBs due to their higher theoretical energy capacity (1494 $mAh.g^{-1}$) compared to current graphite anode materials (372 $mAh.g^{-1}$) [5].

SnO_2 is a semiconductor material with a bandgap of approximately 3.6 eV, and its bandgap can be influenced by the synthesis conditions [6]. Moreover, variations in electronic properties, such as the bandgap, also impact the electrical conductivity and consequently, its battery performance [7]. Therefore, investigating the relationship between the bandgap and electrochemical properties could be a focus of future studies.

In this thesis, the focus is on studying the electronic properties of SnO_2. SnO_2 nanoparticles were synthesized in the nanotechnology laboratory at the Institute of Forestry and Engineering. The research involves analysing the absorption spectrum of five SnO_2 samples using a UV-Vis spectrophotometer to investigate their absorption behaviour. Understanding the absorption behaviour of SnO_2 is crucial for gaining insights into its electronic properties. The presence of absorption in the visible region indicates the defect states in the material. The UV absorption corresponds to the band-to-band absorption of the material and identifies the bandgap. The electronic properties are the first step in materials characterization. These defect states will also affect the electrochemical performance, which is beyond the scope of this thesis.

1. STATE OF ART

1.1. Batteries

1.1.1. Battery

A battery is a device that stores chemical energy and converts it into electrical energy through a series of electrochemical (redox) reactions. It consists of one or more galvanic cells, where each cell is made up of two electrodes, typically a cathode (positive electrode) and an anode (negative electrode). Electrodes are generally separated by an electrolyte that permits the shuttling of ions. [8]

Batteries can be categorized into two groups, primary batteries, and secondary batteries (Figure 1.1), also known as rechargeable batteries. Primary batteries are used for low-cost consumer goods and have single use only, making them disposable. In primary batteries, also known as dry cells, an irreversible chemical reaction occurring between the electrodes and electrolyte causes a permanent change, explaining the non-rechargeable character. For example, the most famous primary batteries are zinc-carbon and alkaline batteries. The basic construction of a zinc-carbon battery consists of a cylindrical zinc casing as an anode, a carbon rod as a cathode, and an electrolyte paste that separates the two electrodes. The electrolyte paste is typically made of ammonium chloride and zinc chloride, and it helps to conduct electricity between the two electrodes. An alkaline battery shares a similar construction to a zinc-carbon battery, with a cylindrical metal casing that serves as an anode, a carbon rod or mixture of carbon and manganese dioxide as a cathode, and an electrolyte paste that separates the two electrodes. However, the electrolyte paste in an alkaline battery is more efficient and long-lasting compared to that in a zinc-carbon battery. This allows the alkaline battery to provide a more consistent and higher voltage output over its lifespan. [9],[10]

Secondary batteries are known as rechargeable batteries, designed for reusable purposes. Usage of secondary batteries is wide, for example, in smartphones, laptops, electrical

vehicles, and renewable energy systems. In secondary batteries, cells the electrochemical reactions are changeable or reversible and ions accumulate at the electrodes, ready to discharge electricity when they flow back which means they can repeatedly store electrical energy. Among the several types of secondary batteries, lithium-ion batteries (LiBs) are the most widely used. LiBs operate by the movement of lithium ions between the two electrodes, facilitating the storage and release of electrical energy. However, there are other rechargeable battery types available, including nickel-metal hydride (NiMH), nickel-cadmium (Ni-Cd), and lead-acid batteries. [10]

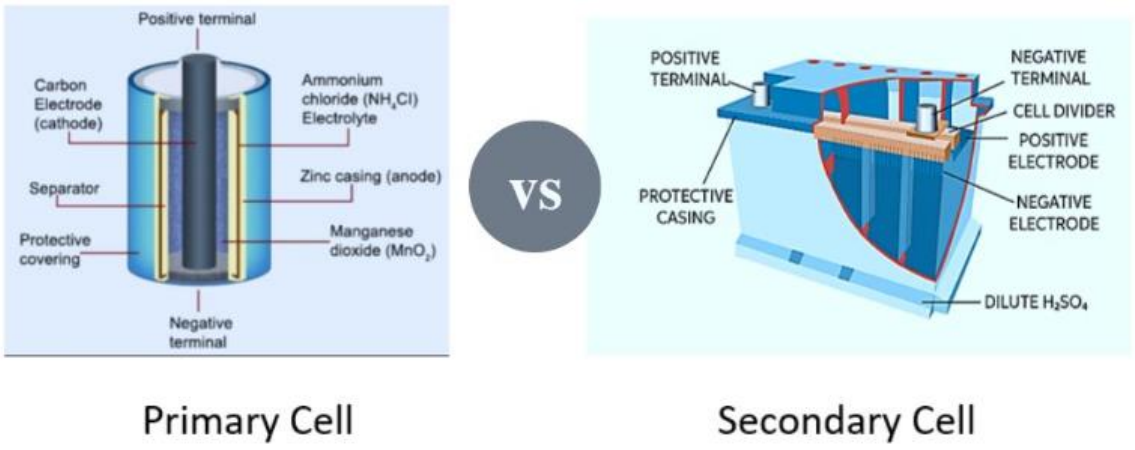

Figure 1.1. Schematic representations of battery types [11].

The process of discharging a battery involves a chemical reaction that occurs within the battery. When a battery is connected to a circuit, a chemical reaction occurs between the electrodes and the electrolyte, creating a flow of electrons from the negative to the positive electrode, generating a flow of electrical energy. This process continues until the battery's chemical energy is fully depleted, and the battery can no longer provide power to the device. The rate of discharge depends on several factors, including the type of battery, the device's power requirements, and the condition of the battery. As the battery discharges, its voltage level drops, and the device may start to operate less efficiently or even shut down if the battery is completely drained. [8],[9] For example a lithium-ion battery in an iPhone® is designed to retain up to 80% of its original capacity after 500 complete charge cycles [12].

1.1.2. Lithium-ion battery

A lithium-ion battery, also known as a Li-ion battery, is a type of rechargeable battery that uses lithium ions as the main charge carriers. In Figure 1.2, an illustration of LiB is displayed, resulting in the stacking of multiple cells, where a cell consists of a cathode and an anode, separated by an electrolyte. The cathode is typically made of a lithium metal oxide such as lithium cobalt oxide, lithium manganese oxide, and lithium nickel manganese cobalt oxide [13] while the anode is usually made of graphite. The electrolyte can be in a liquid or solid state but is commonly a lithium salt (*e.g.*, hexafluorophosphate, perchlorate, tetrafluoroborate, hexafluorophosphate) that is dissolved in an organic solvent, often soaked into a porous separator that is placed between the cathode and anode.

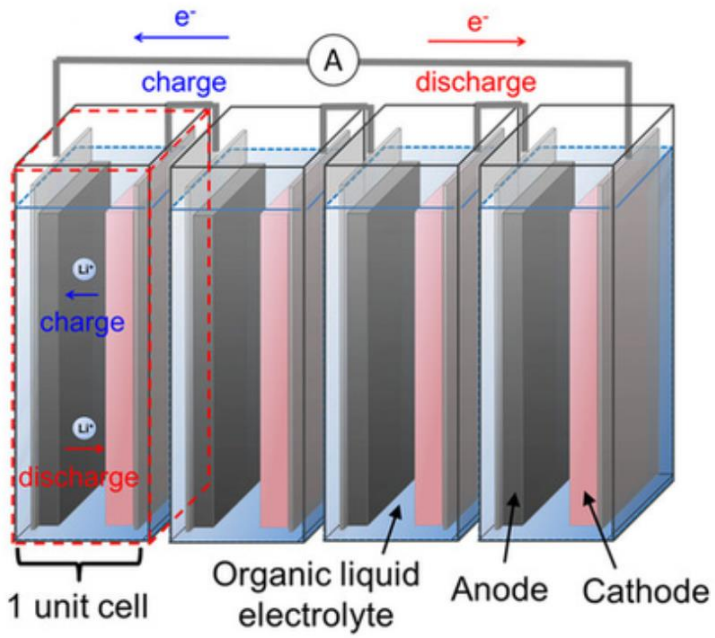

Figure 1.2. Lithium-ion battery scheme, 2015 nature [14].

In a Li-ion battery, spontaneous electrochemical reactions occur in the anode, generating lithium ions originally stored in the graphite anode and releasing a flow of electrons that pass through the external circuit. These electrons aim to help to power the plugged device before recombining with lithium ions at the cathode. The opposite reaction occurs during the charge, an external circuit that provides electricity energy pushes the electrons out of the cathode, inducing a high electron density to the anode which attracts and forces the lithium

ions to move from the cathode back to the anode. Essentially, in the discharge phase, the chemical stored energy is converted into electrical energy, which powers the device. Conversely, during the charging phase, the reverse reaction occurs, where an external electrical source replenishes the battery by regenerating the chemical energy (Figure 1.3). [15]

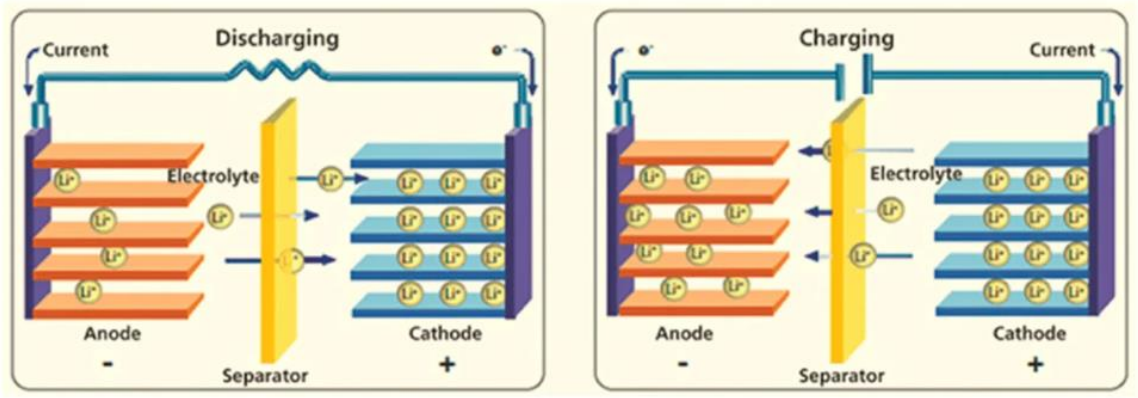

Figure 1.3. Lithium - Ion battery working principle [15].

Li-ion batteries are widely used due to their advantages:

- With high energy density, they can store more energy in each volume or weight compared to other types of batteries, making them ideal for use in portable and mobile devices due to lithium which is a very light element [16].
- High voltage, LiBs have a higher voltage compared to other types of batteries, typically around 4 volts, which allows them to deliver more power and provide longer run times for devices [17].
- With low self-discharge, they lose very little energy when not in use, making them suitable for use in devices that are not used frequently, such as backup power supplies [18].
- LiBs have a relatively acceptable cycle life duration compared to other batteries in the market, making them well-suited for use in devices that are frequently charged and discharged, such as smartphones and laptops [16].
- Due to Li^+ ions' smaller size, they can move more easily through the structure of battery electrodes and can be stored more densely in the anode compared to sodium-ion batteries, where Na^+ ions are larger and require more space to move around [19].

- LiBs can be in several different varieties such as lithium-cobalt, lithium-manganese [20] lithium-sulphur, and silicon because their very light weight makes them perfect composite to anode material [21], thus making them well suited for use in a wide range of portable and mobile devices, electric vehicles, and renewable energy systems [17].

Li-ion batteries are already exceptionally good, but still have many disadvantages:

- Li-ion batteries have a limited lifespan and their capacity to hold a charge decreases over time. This means that they will eventually need to be replaced [22].
- Li-ion batteries have been known to catch fire or explode if they are damaged, overheated, or overcharged. Proper handling and storage of these batteries are essential to minimize the risk of accidents [23].
- Li-ion batteries are still relatively expensive compared to other types of batteries, making them less accessible to consumers and businesses [23].
- The production, and disposal of Li-ion batteries can harm the environment [21]. They contain toxic chemicals like cobalt, nickel, and cadmium that can leach into soil and water if not disposed of properly [23].
- Li-ion batteries are sensitive to temperature changes and can suffer damage or lose capacity if exposed to extreme temperatures [24].
- Li-ion batteries can take longer to charge compared to other types of batteries, which can be an inconvenience for users who need their devices charged quickly [25].
- The capacity of a Li-ion battery can decrease over time, even if it is not used. This is due to a natural process known as capacity fade, which reduces the amount of energy the battery can store [20].

1.2. Electronical properties

1.2.1. Bandgap

The bandgap refers to the energy (Figure 1.4) between the top of the valence band (E_V) and the bottom of the conduction band (E_C). This forbidden part cannot be occupied by electrons; therefore, the bandgap energy (E_G) also describes the minimum energy that an electron requires to jump from the valence band to the conduction band. Many external sources can be the origin of electron excitation, such as heat, a photon, or an electrical field. [26]

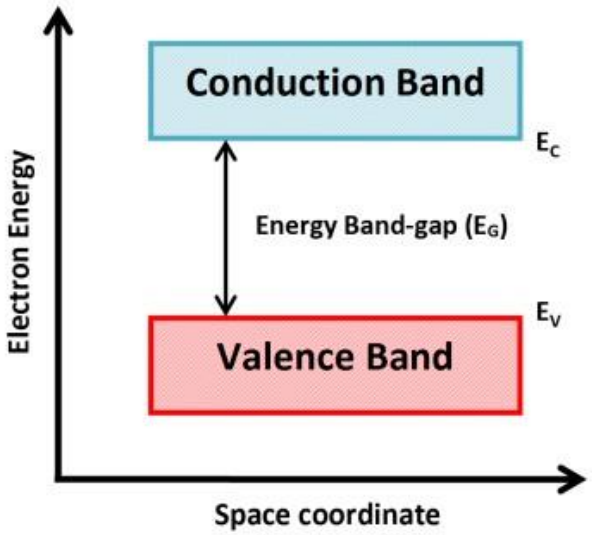

Figure 1.4. Bandgap diagram [26].

In the field of nanotechnology, understanding the bandgap of materials is crucial because their properties can significantly differ when scaled down to the nanoscale. Any changes in the bandgap at this scale can have a direct impact on the materials' characteristics as the size of a material decreases, its bandgap may increase or decrease depending on the specific material and its nanoscale structure.

1.2.2. Types of materials

Materials can be divided into three sub-categories depending on their ability to conduct electrical current: conductors, semiconductors, and insulators.

Conductors are materials that allow electrons to flow easily from atom to atom inside a conducting material when a voltage is applied. This is because the valence band and the conduction band overlap, which means that there is no bandgap between them (Figure 1.5), and electrons can freely move between the two overlapping bands. Metallic materials, such as copper, aluminium, silver, and gold, are considered good conductors. [27]

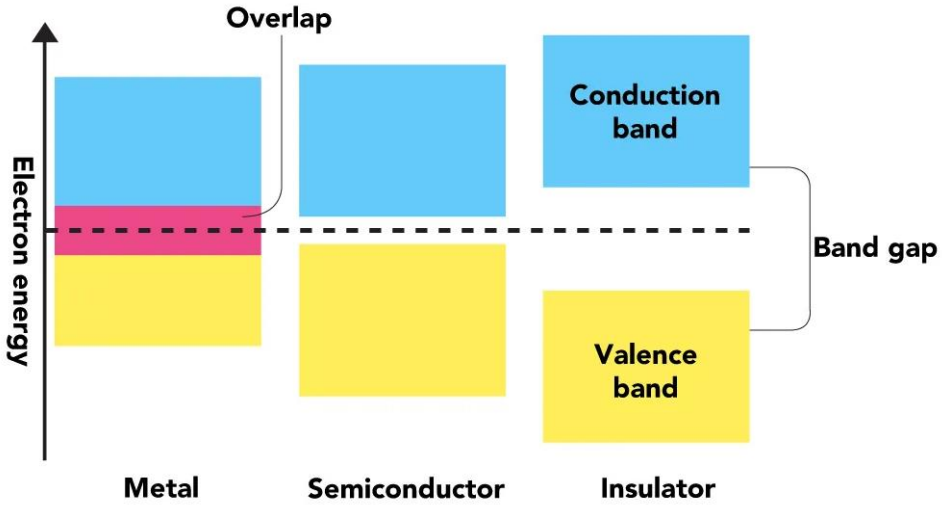

Figure 1.5. The bandgap model [28].

Contrary to conductors, insulators barely not conduct electricity. In the case of an insulator, this bandgap is high (generally above 4 eV). Due to this high energic forbidden region, the electrons are prevented from being promoted from the valence to the conduction band (Figure 1.5). Some examples of insulators include glass, ceramics, plastics, and rubber. [27]

Semiconductor materials are characterized as intermediate materials between conductors and insulators. They have moderate electrical conductivity and bandgap energy between 0 and 4 eV. The most used semiconductors are silicon, germanium, and tin oxide. Semiconductors can also be doped with impurities to enhance their electrical conductivity and modify their electronic properties. For example, silicon can be doped with phosphorus or tin oxide with lead. [27]

Two types of bandgaps exist in semiconductors: direct and indirect. Direct bandgap materials occur when the maximum of the valence band appears to be at the same space momentum as the minimum of the conduction band. The direct transition allows electrons to directly jump from the valence band to the conduction band and releases energy in the form of light. When the maximum of the valence band takes place at a different space momentum from the minimum of the conduction band, it results in an indirect bandgap. Consequently, electrons cannot directly transition to the valence band and must also undergo a phonon-assisted transition, which reduces the probability of the electron transitioning and emitting light. The schematic illustration of bandgap types is shown in Figure 1.6.

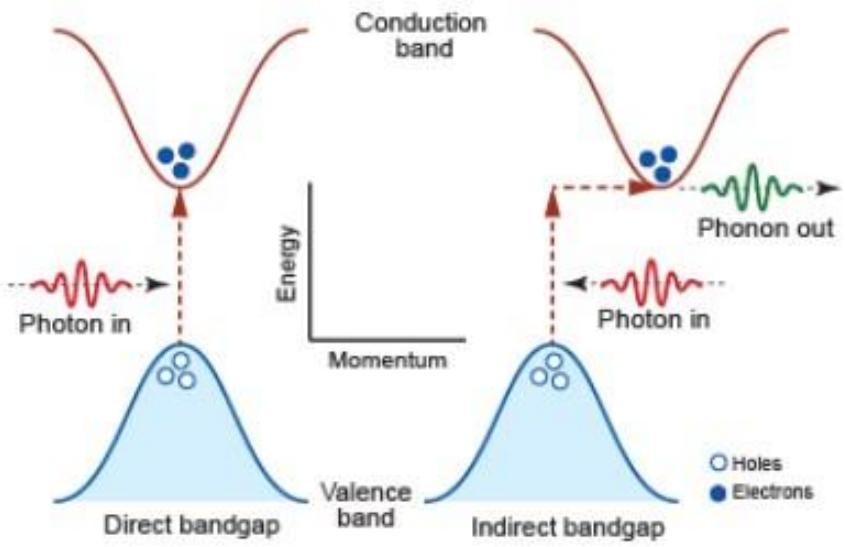

Figure 1.6. Schematic illustration of direct and indirect bandgap semiconductors [29].

The main difference between direct and indirect bandgap materials is that direct bandgap materials are better for light emission and absorption, while indirect bandgap materials are less efficient.

1.2.3. Types of semiconductors

Semiconductors offer several advantages over conductors, including the ability to modify their energy band structures using nanoparticles or dopants. This modification enhances

improving their energy storage capabilities, resulting in faster charging times and improved performance even in extreme temperatures [30].

Semiconductors can be classified into two types based on their conductivity properties: n-type and p-type. To illustrate these types, the silicon (Si) crystal structure is a good example as Si is a widely used semiconductor material with four valence electrons.

The addition of a trivalent impurity such as boron (B), indium (In), or aluminium (Al) into a silicon crystal can only generate three covalent bonds between the impurity and the silicon. However, since the silicon has four electrons, one of the silicon electrons is impaired and creates a hole to compensate for the lack of a bonding electron. The presence of holes in the material contributes to its conductivity and is referred to as a "p-type" semiconductor (Figure 1.7) [31].

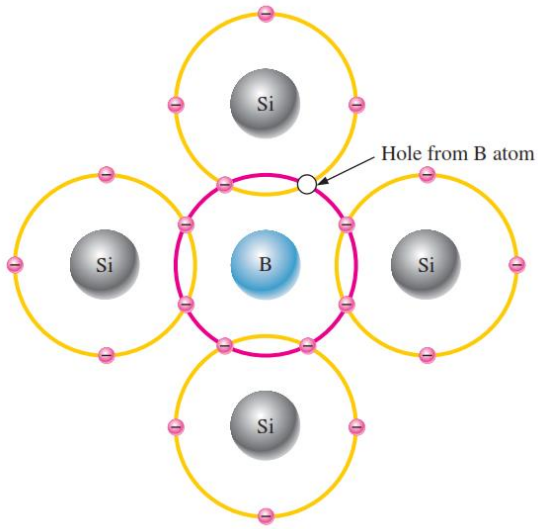

Figure 1.7. P-type semiconductor. Boron (B) impurity atom in a silicon crystal [31].

In an "n-type" semiconductor, an impurity with more electrons is added to the silicon crystal, typically a pentavalent impurity such as phosphorus (P), bismuth (Bi), or antimony (Sb). In this case, one of the electrons from the pentavalent impurity is not involved in bonding with the silicon atom, and it becomes a free electron. These free electrons play a significant role in enhancing the conductivity of the semiconductor (Figure 1.8) [31].

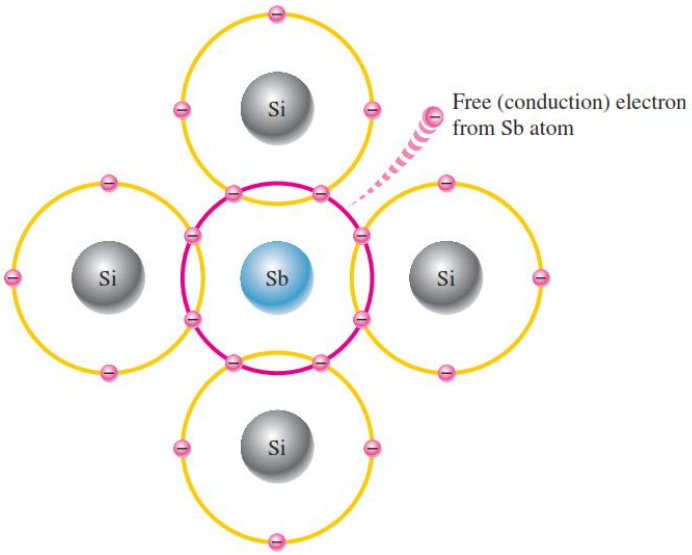

Figure 1.8. N-type semiconductor. Antimony (Sb) impurity atom in a silicon crystal [31].

The amount and type of impurities added to the semiconductor can significantly affect the resulting electrical properties of the material by changing the charge carrier concentration. This makes doping a valuable tool for controlling the electrical properties of semiconductors, which are essential for many electronic devices.

1.3. Nanomaterials

Nanomaterials (NM) is the basis of nanoscience and nanotechnology. NM is defined as a set of substances that have at least one dimension in the nanoscale range, typically between 1 and 100 nanometers (see Figure 1.9). One nanometer is equivalent to one billionth of a meter.

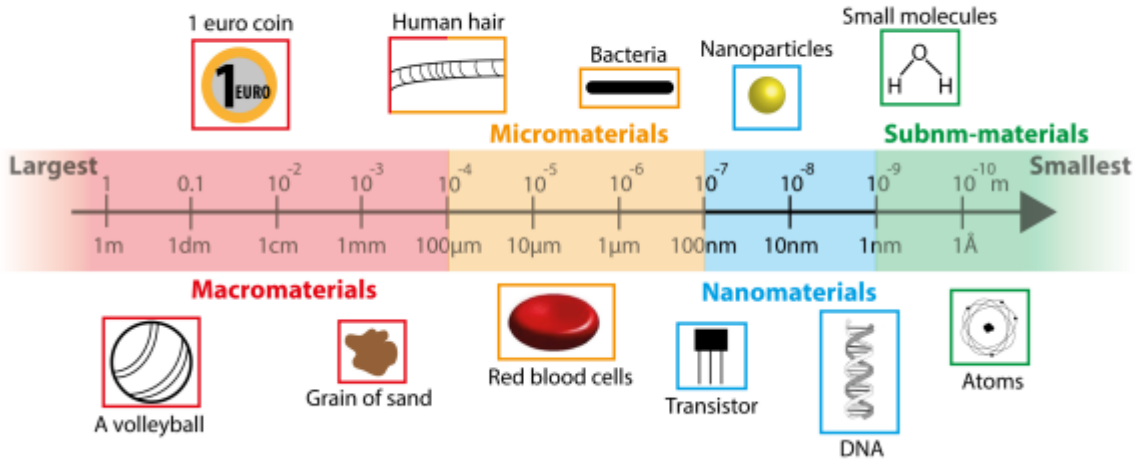

Figure 1.9. Length scale frame of reference for the size of nanoparticles [32].

There exists a diverse array of nanomaterials, including nanoparticles, nanoclusters, quantum dots, nanowires, nanotubes, nanosheets, and graphene. Each of these nanomaterials possesses distinct morphologies, leading to a wide range of properties and potential applications. Through careful synthesis, the size and shape of nanomaterials can be precisely controlled, allowing for the customization and optimization of properties specific to desired applications. The nanoscale size of these materials confers unique and outstanding physical, chemical, and biological properties that are not present in bulk materials. [33]

1.3.1. Applications of nanomaterials

Nanomaterials have a wide range of applications, from medicine to electronics, but also in energy and the environment [34]. For instance, nanomaterials are already used as drug delivery or imaging agents in medicine [35], they can also be incorporated in transistors and

sensors to enhance their performances in electronics [36]. They have also provided efficiency for the environment since they can be used for water treatment [37], air filtration [38], or soil remediation [39]. In addition to battery applications, nanomaterials are widely investigated and exploited for energy production (*e.g.*, solar and fuel cells).

1.3.2. Nanomaterials in lithium-ion batteries

Nanomaterials are a key area of research and development especially in the field of batteries since the storage of electrical energy is becoming every year increasingly important. They are present in our daily life, for example in portable devices (smartphones, laptops, smart watches), electric vehicles, and grid energy storage systems. Nanomaterials in LiBs can improve the energy capacity and density of the electrodes, for instance, the use of tin-based nanoparticles such as stannic oxide (SnO_2), stannous sulphide (SnS) and stannic sulphide (SnS_2) as anode materials can provide higher capacity compared to traditional graphite, owing to their ability to undergo multiple electrochemical reactions [40].

Silicon anodes demonstrate exceptional theoretical energy capacity (4200 $mAh.g^{-1}$). Moreover, they exhibit high-rate performance, enabling rapid charging and discharging, which is important for applications that require high power output like electric vehicles [41]. However, silicon also suffers from poor conductivity and large volume changes during the charging and discharging process, which causes mechanical internal stress and can lead to cracking and degradation of the electrode, ultimately resulting in poor cycling stability [42]. Although silicon is abundant, its manufacturing requires high melting temperatures, leading to significant energy consumption and increased production costs [43].

In contrast, tin offers a lower theoretical capacity compared to silicon but can still deliver reliable performance as an anode material. It undergoes smaller volume changes during charging and discharging compared to silicon and relatively high conductivity which can result in an improved performance and cycling stability. Tin raw materials and processing also have a considerably lower cost compared to silicon, making it a more economically viable option to use in energy storage applications [44].

1.4. SnO_2 nanomaterials

1.4.1. Stannic oxide (SnO_2)

SnO_2, also called stannic oxide, is crystalline and exhibits, specifically the tetragonal rutile crystal structure. The unit cell of SnO_2 consists of two tin (Sn) atoms and four oxygen (O) atoms. Each Sn atom is located amidst 6 oxygen atoms at its corner and almost forms a mixture of corner and edge-sharing regular octahedra. The unit cell is a tetragonal prism as shown in Figure 1.10 [45].

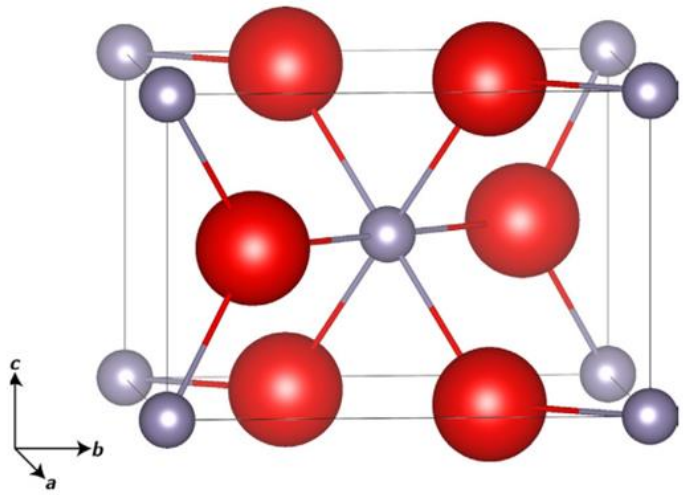

Figure 1.10. SnO_2 unit cell, with Sn shown in grey and O in red [45].

Non-stoichiometry between Sn and O atoms is responsible for the n-type semiconductor properties, especially the presence of natural oxygen vacancies (some oxygen atoms missing in the crystal). The lack of oxygen is reported as being the main reason for free electron generation. [46] In addition to energy storage technologies applications, SnO_2 materials have been thoroughly investigated as gas sensors, spintronics, and photocatalysis applications.

1.4.2. Electrochemical properties of SnO_2

SnO_2-based nanomaterials are being considered as a replacement for graphite in lithium-ion battery anodes. This is because they are low-cost, environmentally friendly, and have a high theoretical capacity of 1494 $mAh.g^{-1}$, which is about four times higher than graphite. The process of using SnO_2 in battery anode electrodes typically involves two distinct chemical reactions. First, SnO_2 is converted into metallic Sn particles and a Li_2O matrix, the process is generally considered irreversible for bulk SnO_2, and then, the freshly formed Sn particles are alloyed with Li^+ ions.

The theoretical capacity of SnO_2 can reach 783 $mAh.g^{-1}$ based on the alloying reaction alone, and up to 1494 $mAh.g^{-1}$ if the first reaction is completely reversible [47]. However, SnO_2 undergoes a significant volume change during charge and discharge cycles which leads to capacity fading over time. The study by Hu et al. [48], has shown that using SnO_2 nanoparticles with sizes below 11 nm can prevent capacity loss and irreversibility issues that may arise in larger particles.

2. AIM AND OBJECTIVES

The main aim of this bachelor thesis is to investigate the influence of the SnO_2 synthesis conditions on electronic and optical properties by understanding the effect of synthesis temperature and duration on SnO_2 bandgap and small absorptions using UV-Vis spectroscopy.

To achieve this aim, the following sub-steps will be taken:

1. Measure the UV-vis spectra of each SnO_2 sample previously synthesized under different time and temperature conditions.
2. Analyse the spectra to determine the bandgap of SnO_2 and for small absorptions effects in SnO_2 under each synthesis condition.
3. Compare the bandgaps and absorptions of SnO_2 synthesized under different time and temperature conditions to find any trends or correlations.
4. To explore the different synthesis conditions and analyse their respective effects on the resulting bandgaps of SnO_2.

By achieving these objectives, this thesis goal is to evaluate the role of synthesis conditions on the bandgap and defect states. This will enable us to choose SnO_2 with the best synthesis conditions (time and temperature) for further studies, particularly in the field of electrochemical characterization.

3. EXPERIMENTAL PART

3.1. Materials

SnO_2 samples were synthesized beforehand using the same protocol. *i.e.*, the same precursor solvent and reactant were used for all syntheses. However, synthesis temperature and duration were varied to produce samples that have potentially different properties. The specific synthesis conditions employed are provided in Table 1. The synthesis process used white SnO_2 powder, which was subsequently subjected to appropriate treatments and later analysed in the study.

Table 1. An exhaustive list of samples

Label	Synthesis temperature (°C)	Synthesis duration (h)
T190-20	190	20
T190-15	190	15
T190-10	190	10
T190-06	190	6
T250-06	250	6

These nanomaterials are individually treated for next purposes, such as UV-visible spectroscopy measurement in this study or electrochemical characterization in another study.

3.2. UV-Vis spectroscopy

3.2.1. Principle

UV-Vis spectroscopy is a technique used to analyse the absorption or transmission of light in the ultraviolet (UV) and visible (Vis) regions of the electromagnetic spectrum (Figure 3.1). This refers to the quantitative measurement of the absorbed light of a sample using discrete wavelengths of UV and Vis light. UV part is attributed to be between 10 and 380 nm, while

visible light is approximately ranging from 380 to 780 nm. The amount of absorbed light is compared to a reference or blank sample. The amount of light absorbed or transmitted at each wavelength provides information about the sample's electronic structure and composition [49].

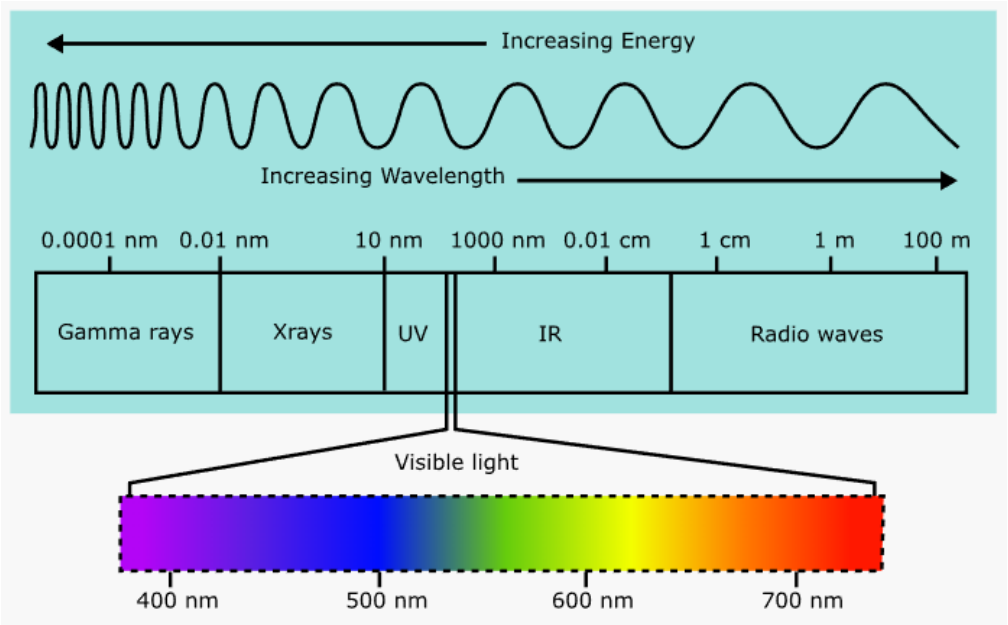

Figure 3.1. Electromagnetic spectrum [49].

The working principle of UV-Vis spectroscopy as shown in Figure 3.2 is that a beam of light is passed through a sample and measuring the amount of light absorbed as a function of wavelength. The resulting spectrum is compared to a blank sample, and the comparison provides insight into the electronic transitions taking place in the sample. The energy difference between electronic states determines which wavelengths of light are absorbed by the sample, revealing information about its electronic structure.

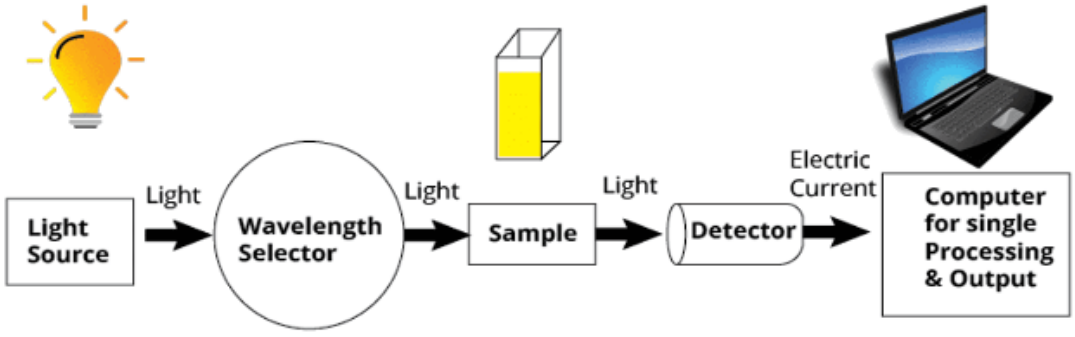

Figure 3.2. Representation of Working of the UV-Vis Spectrophotometry [50].

The absorbed radiation is the difference between the initial radiation (I_0) and the transmitted radiation (I). The amount of absorbed radiation is known as absorbance (A), and transmittance (T) is a fraction (I/I_0) representing the amount of light that passes through the sample. Transmittance and absorbance can be explained as an equation [50]:

$$T = \frac{I}{I_0} \tag{3.1}$$

The UV-Vis spectrophotometer primarily measures transmittance values but can also calculate absorbance values by taking the negative logarithm of the transmittance. Absorbance is a unitless quantity commonly used to quantify the amount of light absorbed by a sample.

$$A = -log_{10}T \tag{3.2}$$

The spectrophotometer measures the intensity of incident radiation (I_0) before it passes through the sample and the intensity of transmitted radiation (I) that has passed through the sample. By comparing these two intensities, it provides the absorbance value (A or Abs).

3.2.2. Sample preparation and measurement

Sample powders are initially ground and a small amount of each sample (a few milligrams) is then dispersed in 5 ml of isopropanol. The dispersions are manually agitated and then sonicated in an ultrasonic bath for 5 minutes. However, due to the rapid precipitation of the powder, quantitative measurements cannot be conducted as the exact concentration in the solution is unknown. Instead, a few millimetres of each dispersion are poured into UV-visible cells (VWR®) and analyzed by UV-visible spectroscopy.

Absorption spectra were recorded using instrument a VWR UV-1600PC, UV-visible spectrophotometer as shown in Figure 3.3. It is capable of measuring absorption with the accuracy of ±0.50 nm and the suitable wavelength range for measurements is 190-1100 nm. Measurements were made in the range of 250 – 900 nm with a resolution of 2 nm.

Figure 3.3. VWR UV-1600PC, UV-Visible Spectrophotometer.

Direct and indirect allowed transition bandgap energies were estimated using the Tauc plot and calculated from absorption spectra obtained by UV-visible measurements.

3.2.3. Tauc plot

A Tauc plot is a commonly used graphical technique in materials science and condensed matter physics for determining the bandgap of a semiconductor material.

A semiconductor material is expected to show no photon absorption below the bandgap, with a sudden increase in absorption once the bandgap is reached. Therefore, in a UV-visible spectrum, the bandgap is identified as the point where the absorption begins to rise, showing

the minimum energy required to promote an electron from the valence band to the conduction band.

Optical bandgap can be calculated using the Tauc relation as equation 3.3:

$$\alpha h\nu = A(h\nu - E_g)^n \tag{3.3}$$

A is a constant, h is Planck's constant (6.63 10^{-34} m^2.kg/s) and ν is the frequency of the photon and n is an exponent that depends on the nature of the semiconductor material. For direct bandgap semiconductors, n is typically 1/2, while for indirect bandgap semiconductors, n is equal to 2. The frequency of the photon can be calculated from the photon wavelength (or related energy) as described in equation 3.4:

$$E = h\nu = \frac{hc}{\lambda} \tag{3.4}$$

E is the energy of the photon (eV or J), h is Planck's constant, c is the speed of light in a vacuum (3.0 10^8 m/s) and λ is the photon wavelength (m).

To construct a Tauc plot, the absorption coefficient (α) of a semiconductor material is first measured using UV-Vis spectroscopy. Then, $(\alpha h\nu)^{1/n}$ graphs are plotted as a function of photon energy hν depending on the n value, *i.e.*, n is equal to 1/2 or 2 for direct and indirect bandgap, respectively. By extrapolating the linear part of the Tauc plot to the x-axis, the bandgap can be determined.

4. RESULTS AND DISCUSSION

The data obtained from the spectrophotometer was collected, plotted using Origin, and then thoroughly analyzed.

4.1. Influence of synthesis duration

Figure 4.1 shows the absorption spectra of four samples with the same temperature, but different synthesis duration. All samples prove a similar tendency with a peak between 276 to 280 nm. The exact wavelength value of each peak is listed in Table 2. In addition to this, the UV-Vis spectra show transparent behaviour in the visible light range. However, as the powder where not weight beforehand, absorption intensity values cannot be compared.

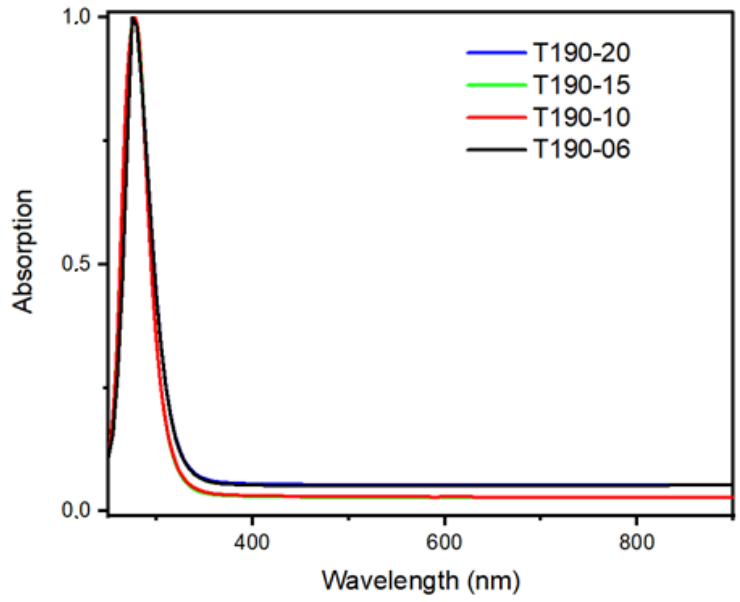

Figure 4.1. Absorption spectra of four samples.

It seems that the influence of the synthesis duration has no impact on the biggest absorption peak wavelength. The difference between the maximum and minimum peak wavelengths corresponds to the UV-Vis spectrum resolution, therefore, the shift is negligible.

Table 2. Peaks wavelength values of the different samples

Label	Absorption peak wavelength (nm)
T190-06	276
T190-10	278
T190-15	276
T190-20	276

Figure 4.2. illustrates the Tauc plots used to determine the direct and indirect bandgaps and their variations in four samples. The direct bandgap values range from 4.12 eV to 4.19 eV (Figure 4.2.a), while the indirect bandgap values range from 3.65 eV to 3.80 eV (Figure 4.2.b). These calculations offer valuable insights into the range of bandgaps associated with the direct and indirect transitions observed in the analysed samples.

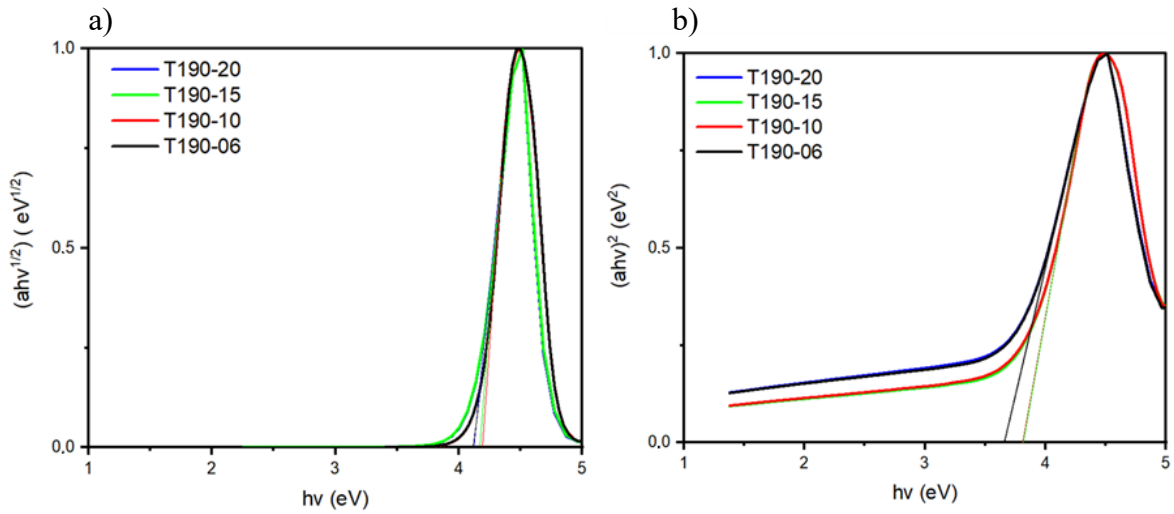

Figure 4.2. Tauc plot of a) direct and b) indirect bandgap of four samples.

The direct bandgap is higher than usual and referenced SnO_2 materials. However, further characterizations need to be performed to understand the chemical and physical properties of studied samples.

The influence of synthesis duration has been investigated on direct and indirect bandgap and is resumed in Table 3.

Table 3. Direct and indirect bandgap values of the different samples

Label	Direct bandgap (eV)	Indirect bandgap (eV)
T190-06	4.12	3.65
T190-10	4.19	3.80
T190-15	4.17	3.80
T190-20	4.12	3.65

The variations in bandgap values are depicted in Figure 4.3. It can be observed that the error bars for the direct gap of SnO_2 samples overlap, indicating that the influence of synthesis duration is insignificant. Error margins were arbitrarily estimated at 10 % of the respective bandgap value. However, a noticeable trend can be observed for the indirect bandgap (Figure 4.3). The indirect bandgap increases from 3.65 eV for the T190-06 sample to 3.80 eV for the T190-10 sample. Subsequently, with a further increase in synthesis time, the indirect bandgap decreases from 3.80 eV to 3.65 eV.

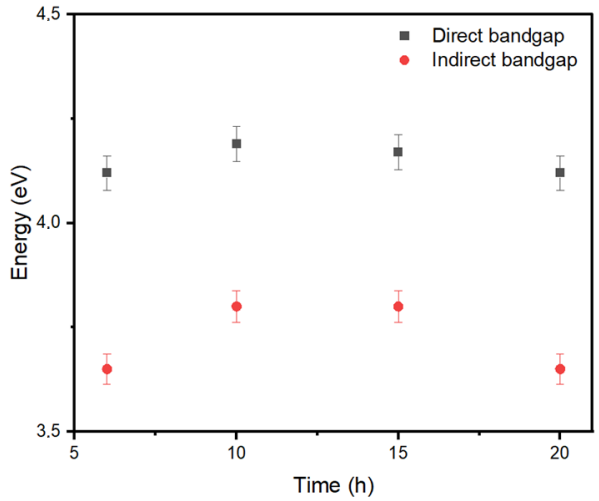

Figure 4.3. Influence of synthesis time on direct and indirect bandgap.

UV-visible spectra of all samples exhibit small absorption peaks in the visible range. Specifically, Figure 4.4 illustrates the absorption spectra of the T190-10 sample, which reveals three absorption peaks at 450 nm, 560 nm, and 600 nm. These peaks are likely attributed to defect states, as their corresponding energies are below the bandgap values of 4.19 eV and 3.80 eV for the direct and indirect bandgaps, respectively.

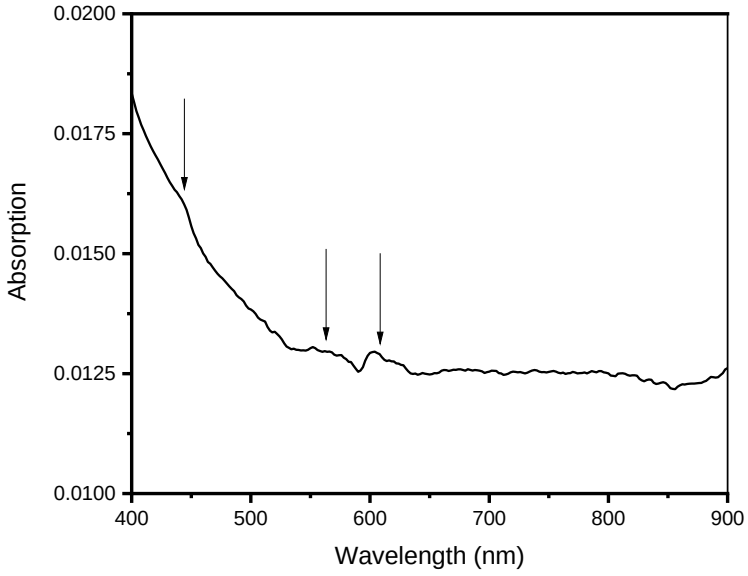

Figure 4.4. Visible absorption of T190-10 sample.

Table 4 provides a summary of the presence of absorption peaks in the visible range for different synthesis times of SnO_2 samples. It indicates that a longer synthesis time, such as 20 hours (T190-20), results in a higher number of defects compared to a sample synthesized for 6 hours (T190-06). However, it should be noted that the intensities of the absorption peaks cannot be precisely measured as the powders were not weighed before the analysis.

Table 4. Defect states the presence of the different samples

Wavelength (nm) energy (eV)	450 2.8	560 2.2	600 2.1	680 1.8	760 1.6
T190-06	✓				
T190-10	✓	✓	✓		
T190-15	✓	✓	✓		✓
T190-20	✓	✓	✓	✓	✓

The presence of defect states in the SnO_2 samples may indeed contribute to the observed variations in the indirect bandgap. Further investigations are required to confirm the existence of these detected defect states and to assess their impact on other material properties. These additional studies will provide a more comprehensive understanding of the role of defects in the synthesized SnO_2 samples.

4.2. Influence of synthesis temperature

Figure 4.4 shows the absorption spectra of the T250-06 sample, which gives a similar curve compared to the T190-06 sample. There are no noticeable differences in the wavelengths of the absorption peaks between the two samples. The difference in absorption intensity is caused by non-quantitative measurements, as powder weight was not measured before dispersion.

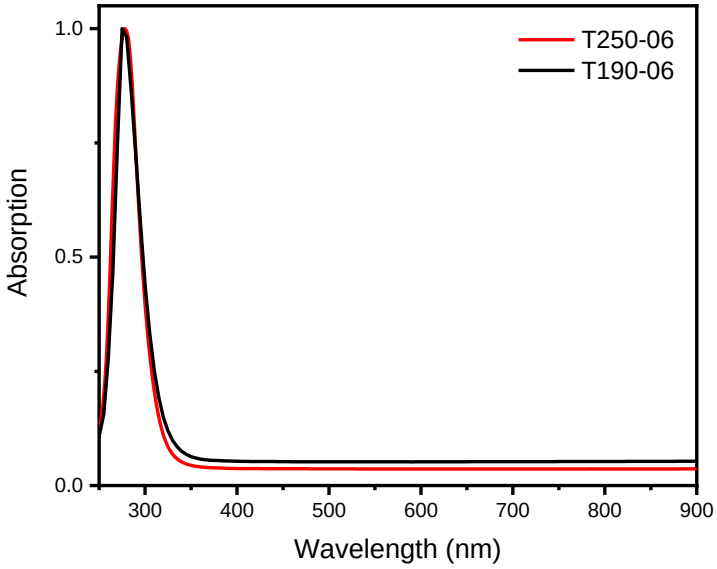

Figure 4.4. Absorption spectra of T190-06 and T250-06 samples.

The influence of synthesis temperature on the direct and indirect bandgap has been investigated using the Tauc plot, as shown in Figure 4.5. A slight increase in the direct bandgap is observed between the T190-06 sample (4.12 eV) and the T250-06 sample (4.16 eV). Similarly, an increase is noticed in the indirect bandgap as the temperature is increased, with the T190-06 sample having a bandgap of 3.64 eV and the T250-06 sample having a bandgap of 3.78 eV.

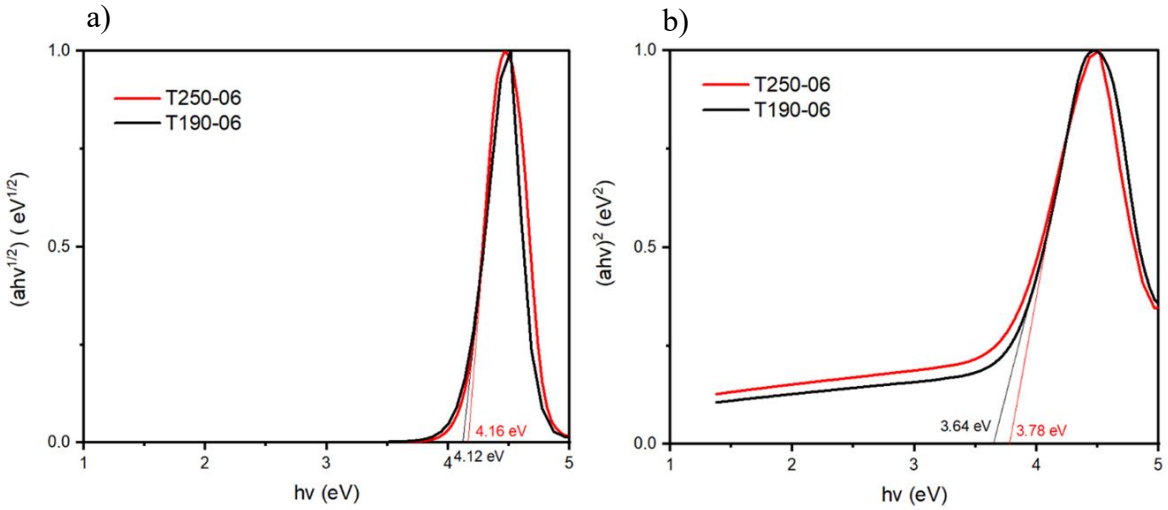

Figure 4.5. Tauc plot of a) direct and b) indirect bandgap of T250-06 and T190-06 samples.

Complementary measurements are essential to gain a comprehensive understanding of the observed tendency in the indirect bandgap. These additional measurements can provide insights into numerous factors that may influence the bandgap, such as defect states, size, morphology or structural characteristics.

CONCLUSION

The main goal of this thesis was to employ UV-visible spectroscopy analyses to investigate the electronic properties of five distinct samples of SnO_2 nanomaterials and determine their bandgap. The specific aim was to study how temperature and synthesis time impact the SnO_2 bandgap using the Tauc plot calculations, with the results plotted by Origin software. In conclusion, the direct bandgap did not vary with changes in temperature or synthesis duration, whereas the indirect bandgap was observed to be influenced by both factors.

Synthesis duration was found to affect the indirect bandgap, with values ranging from 3.65 eV to 3.80 eV. Increasing the synthesis time from 15 to 20 hours resulted in a decrease in the indirect bandgap from 3.80 eV to 3.65 eV. The duration of synthesis did not appear to have a significant effect on the absorption spectra, as all samples showed a similar tendency with a peak between 276 to 280 nm, regardless of the synthesis duration. Slight variations in the defect states of SnO_2 were observed in the visible absorption spectra as the synthesis time increased. Longer synthesis times resulted in the creation of more defect levels in the material. For instance, the SnO_2 sample synthesized for 20 hours exhibited a more prominent transition from a defect state compared to the sample synthesized for 6 hours under identical conditions. However, due to the lack of pre-weighed SnO_2 powder, the comparison of absorption intensity values is not possible.

Similarly, variations in synthesis temperature influenced the bandgap. Increasing the temperature from 190 to 250 °C led to a higher bandgap of 4.16 eV for the latter sample, compared to 4.12 eV for the former. However, unlike the synthesis duration, no significant difference was detected in the absorption spectra between the samples synthesized at different temperatures, as they all showed similar values.

Furthermore, the direct bandgap values of the SnO_2 samples showed that variations in synthesis duration and temperature had a negligible effect, with bandgap values ranging from 4.12 eV to 4.19 eV.

However, as this thesis focused on the electronic properties of the synthesized SnO_2 nanomaterials, the observation of defects in the visible range allowed for the identification of the SnO_2 nanomaterial sample with the fewest defect states (T190-06), making it an ideal candidate for further comprehensive investigation in future research. It is important to

acknowledge that the electrochemical performance, which can be influenced by these defect states, falls outside the scope of this thesis. Therefore, additional complementary analyses are necessary to gain a deeper understanding of the synthesized SnO_2 nanomaterials, including exploring their electrochemical behaviour and its correlation with the observed defect states.

REFERENCES

[1] B. Diouf and R. Pode, "Potential of lithium-ion batteries in renewable energy," *Renew. Energy*, vol. 76, pp. 375–380, Apr. 2015, doi: 10.1016/J.RENENE.2014.11.058.

[2] A. Manthiram, A. Vadivel Murugan, A. Sarkar, and T. Muraliganth, "Nanostructured electrode materials for electrochemical energy storage and conversion," *Energy Environ. Sci.*, vol. 1, no. 6, pp. 621–638, Dec. 2008, doi: 10.1039/B811802G.

[3] B. Huang, Z. Pan, X. Su, and L. An, "Tin-based materials as versatile anodes for alkali (earth)-ion batteries," *J. Power Sources*, vol. 395, pp. 41–59, Aug. 2018, doi: 10.1016/J.JPOWSOUR.2018.05.063.

[4] R. B. Rajput and R. B. Kale, "Hydro/solvothermally synthesized visible light driven modified SnO2 heterostructure as a photocatalyst for water remediation: A review," *Environ. Adv.*, vol. 5, p. 100081, Oct. 2021, doi: 10.1016/J.ENVADV.2021.100081.

[5] J. Lin *et al.*, "Graphene nanoribbon and nanostructured SnO2 composite anodes for lithium ion batteries," *ACS Nano*, vol. 7, no. 7, pp. 6001–6006, Jul. 2013, doi: 10.1021/nn4016899.

[6] J. Mayandi, M. Marikkannan, V. Ragavendran, and P. Jayabal, "Hydrothermally Synthesized Sb and Zn Doped Sno2 Nanoparticles," *J. Nanosci. Nanotechnol.*, 2014.

[7] G. F. Dewald, S. Ohno, J. G. C. Hering, J. Janek, and W. G. Zeier, "Analysis of Charge Carrier Transport Toward Optimized Cathode Composites for All-Solid-State Li−S Batteries," *Batter. Supercaps*, vol. 4, no. 1, pp. 183–194, Jan. 2021, doi: 10.1002/BATT.202000194.

[8] "Battery | electronics | Britannica." https://www.britannica.com/technology/battery-electronics (accessed Mar. 25, 2023).

[9] "How do batteries work? A simple introduction - Explain that Stuff." https://www.explainthatstuff.com/batteries.html#howwork (accessed Mar. 25, 2023).

[10] "Types of Secondary Batteries | Electricity - Magnetism." https://www.electricity-magnetism.org/electric-battery/types-of-secondary-batteries/ (accessed Mar. 26, 2023).

[11] "Difference Between Primary Cell and Secondary Cell." https://thechemistrynotes.com/difference-between-primary-cell-and-secondary-cell/ (accessed Apr. 17, 2023).

[12] Y. Sun, L. Kong, H. Abbas Khan, and M. G. Pecht, “Li-ion Battery Reliability - A Case Study of the Apple iPhone®,” *IEEE Access*, vol. 7, pp. 71131–71141, 2019, doi: 10.1109/ACCESS.2019.2918401.

[13] M. K. Shobana, “Metal oxide coated cathode materials for Li ion batteries – A review,” *J. Alloys Compd.*, vol. 802, pp. 477–487, Sep. 2019, doi: 10.1016/J.JALLCOM.2019.06.194.

[14] Y. Gambe, Y. Sun, and I. Honma, “Development of Bipolar All-solid-state Lithium Battery Based on Quasi-solid-state Electrolyte Containing Tetraglyme-LiTFSA Equimolar Complex,” *Sci. Rep.*, vol. 5, Mar. 2015, doi: 10.1038/SREP08869.

[15] N. Chawla, N. Bharti, and S. Singh, “Recent Advances in Non-Flammable Electrolytes for Safer Lithium-Ion Batteries,” *Batter. 2019, Vol. 5, Page 19*, vol. 5, no. 1, p. 19, Feb. 2019, doi: 10.3390/BATTERIES5010019.

[16] M. Gao *et al.*, “Lithium metal batteries for high energy density: Fundamental electrochemistry and challenges,” *J. Energy Chem.*, vol. 59, pp. 666–687, Aug. 2021, doi: 10.1016/J.JECHEM.2020.11.034.

[17] Y. Wang, E. Wang, X. Zhang, and H. Yu, “High-Voltage ‘Single-Crystal’ Cathode Materials for Lithium-Ion Batteries,” 2021, doi: 10.1021/acs.energyfuels.0c03608.

[18] P. Wu *et al.*, “Long cycle life, low self-discharge carbon anode for Li-ion batteries with pores and dual-doping,” *J. Alloys Compd.*, vol. 802, pp. 620–627, Sep. 2019, doi: 10.1016/J.JALLCOM.2019.06.233.

[19] Y. Xu *et al.*, “Electrochemical Performance of Porous Carbon/Tin Composite Anodes for Sodium-Ion and Lithium-Ion Batteries,” *Adv. Energy Mater.*, vol. 3, no. 1, pp. 128–133, Jan. 2013, doi: 10.1002/AENM.201200346.

[20] “BU-205: Types of Lithium-ion - Battery University.” https://batteryuniversity.com/article/bu-205-types-of-lithium-ion (accessed Mar. 30, 2023).

[21] “BU-212: Future Batteries - Battery University.” https://batteryuniversity.com/article/bu-212-future-batteries (accessed Mar. 30, 2023).

[22] P. K. D. Pramanik, S. Pal, and P. Choudhury, “Green and sustainable high-performance computing with smartphone crowd computing: Benefits, enablers, and challenges,” *Scalable Comput.*, vol. 20, no. 2, pp. 259–284, Jun. 2019, doi: 10.12694/SCPE.V20I2.1517.

[23] D. Deng, “Li-ion batteries: Basics, progress, and challenges,” *Energy Sci. Eng.*, vol. 3, no. 5, pp. 385–418, Sep. 2015, doi: 10.1002/ESE3.95.

[24] S. Ma *et al.*, “Temperature effect and thermal impact in lithium-ion batteries: A review,”

Prog. Nat. Sci. Mater. Int., vol. 28, no. 6, pp. 653–666, Dec. 2018, doi: 10.1016/J.PNSC.2018.11.002.

[25] M. J. Lain and E. Kendrick, "Understanding the limitations of lithium ion batteries at high rates," *J. Power Sources*, vol. 493, p. 229690, May 2021, doi: 10.1016/J.JPOWSOUR.2021.229690.

[26] Fayyaz Asad, "(PDF) Performance and robustness characterisation of SiC power MOSFETs," Jul. 2018. https://www.researchgate.net/publication/326392057_Performance_and_robustness_characterisation_of_SiC_power_MOSFETs (accessed Apr. 05, 2023).

[27] "What is a conductor?" https://www.techtarget.com/whatis/definition/conductor (accessed Apr. 03, 2023).

[28] "Why Does Conductivity Increase With Temperature In Semiconductors? | Atlas Scientific." https://atlas-scientific.com/blog/why-does-conductivity-increase-with-temperature-in-semiconductors/ (accessed Apr. 07, 2023).

[29] "(PDF) The CES EduPack DB for Bulk Functional Materials." https://www.researchgate.net/publication/281712335_The_CES_EduPack_DB_for_Bulk_Functional_Materials (accessed Apr. 28, 2023).

[30] Y. Liu, L. Chen, H. Jiang, and C. Li, "Confined Synthesis of SnO2 Nanoparticles Encapsulated in Carbon Nanotubes for High-Rate and Stable Lithium-Ion Batteries," *J. Electron. Mater.*, vol. 51, no. 12, pp. 6637–6644, Dec. 2022, doi: 10.1007/S11664-022-09975-Z/FIGURES/5.

[31] "Difference between N and P Type Semiconductors - The Engineering Knowledge." https://www.theengineeringknowledge.com/difference-between-n-and-p-type-semiconductors/ (accessed Jun. 05, 2023).

[32] B. W. Thesis, "(PDF) Development, synthesis and characterization of multifunctional nanomaterials." https://www.researchgate.net/publication/263723744_Development_synthesis_and_characterization_of_multifunctional_nanomaterials (accessed Apr. 08, 2023).

[33] Z. Vaseghi and A. Nematollahzadeh, "Nanomaterials," *Green Synth. Nanomater. Bioenergy Appl.*, pp. 23–82, Aug. 2020, doi: 10.1002/9781119576785.CH2.

[34] I. Khan, K. Saeed, and I. Khan, "Nanoparticles: Properties, applications and toxicities," *Arab. J. Chem.*, vol. 12, no. 7, pp. 908–931, Nov. 2019, doi: 10.1016/J.ARABJC.2017.05.011.

[35] C. Burda, X. Chen, R. Narayanan, and M. A. El-Sayed, “Chemistry and properties of nanocrystals of different shapes,” *Chem. Rev.*, vol. 105, no. 4, pp. 1025–1102, Apr. 2005, doi: 10.1021/CR030063A.

[36] Y. Wang *et al.*, “Lithium and lithium ion batteries for applications in microelectronic devices: A review,” *J. Power Sources*, vol. 286, pp. 330–345, Jul. 2015, doi: 10.1016/J.JPOWSOUR.2015.03.164.

[37] K. K. Singh, A. Singh, and S. Rai, “A study on nanomaterials for water purification,” *Mater. Today Proc.*, vol. 51, pp. 1157–1163, Jan. 2022, doi: 10.1016/J.MATPR.2021.07.116.

[38] Q. Geng, H. Wang, R. Chen, L. Chen, K. Li, and F. Dong, “Advances and challenges of photocatalytic technology for air purification,” *Natl. Sci. Open*, vol. 1, no. 2, p. 20220025, Apr. 2022, doi: 10.1360/NSO/20220025.

[39] M. L. Del Prado-Audelo, I. García Kerdan, L. Escutia-Guadarrama, J. M. Reyna-González, J. J. Magaña, and G. Leyva-Gómez, “Nanoremediation: Nanomaterials and Nanotechnologies for Environmental Cleanup,” *Front. Environ. Sci.*, vol. 9, p. 645, Dec. 2021, doi: 10.3389/FENVS.2021.793765/BIBTEX.

[40] A. Eftekhari, “Low voltage anode materials for lithium-ion batteries,” *Energy Storage Mater.*, vol. 7, pp. 157–180, Apr. 2017, doi: 10.1016/J.ENSM.2017.01.009.

[41] F. Ozanam and M. Rosso, “Silicon as anode material for Li-ion batteries,” *Mater. Sci. Eng. B*, vol. 213, pp. 2–11, Nov. 2016, doi: 10.1016/J.MSEB.2016.04.016.

[42] N. Dimov, S. Kugino, and M. Yoshio, “Carbon-coated silicon as anode material for lithium ion batteries: Advantages and limitations,” *Electrochim. Acta*, vol. 48, no. 11, pp. 1579–1587, May 2003, doi: 10.1016/S0013-4686(03)00030-6.

[43] K. Morita and T. Miki, “Thermodynamics of solar-grade-silicon refining,” *Intermetallics*, vol. 11, no. 11–12, pp. 1111–1117, Jan. 2003, doi: 10.1016/S0966-9795(03)00148-1.

[44] Z. Xu, Y. Hou, J. Guo, J. Wang, and S. Zhou, “Metallic Tin Nanoparticle-Reinforced Tin-Doped Porous Silicon Microspheres with Superior Electrochemical Lithium Storage Properties,” *ACS Appl. Energy Mater.*, vol. 4, no. 12, pp. 14141–14154, Dec. 2021, doi: 10.1021/ACSAEM.1C02916/ASSET/IMAGES/LARGE/AE1C02916_0011.JPEG.

[45] J. Savioli, A. L. Gavin, A. K. Lucid, and G. W. Watson, “The structure and electronic structure of tin oxides,” *Tin Oxide Mater.*, pp. 11–39, Jan. 2020, doi: 10.1016/B978-0-12-815924-8.00002-5.

[46] X. Sun, R. Long, X. Cheng, X. Zhao, Y. Dai, and B. Huang, “Structural, electronic, and

optical properties of N-doped SnO2," *J. Phys. Chem. C*, vol. 112, no. 26, pp. 9861–9864, Jul. 2008, doi: 10.1021/JP710564G/ASSET/IMAGES/LARGE/JP-2007-10564G_0001.JPEG.

[47] H. Kim *et al.*, "Comparative study of bulk and nano-structured mesoporous SnO2 electrodes on the electrochemical performances for next generation Li rechargeable batteries," *J. Power Sources*, vol. 413, pp. 241–249, Feb. 2019, doi: 10.1016/J.JPOWSOUR.2018.12.035.

[48] R. Hu *et al.*, "Unveiling critical size of coarsened Sn nanograins for achieving high round-trip efficiency of reversible conversion reaction in lithiated SnO2 nanocrystals," *Nano Energy*, vol. 45, pp. 255–265, Mar. 2018, doi: 10.1016/J.NANOEN.2018.01.007.

[49] "UV-Vis Spectroscopy: Principle, Instrumentation, and Applications - Instrumental Analysis - PSIBERG." https://psiberg.com/uv-vis-spectroscopy/ (accessed Apr. 11, 2023).

[50] "UV Visible Spectroscopy | Learn Important Terms and Concepts." https://www.vedantu.com/chemistry/uv-visible-spectroscopy (accessed Apr. 11, 2023).

ÜLDKOKKUVÕTE

Akud on oluline osa meie igapäevaelust, eriti kaasaskantavate elektroonikaseadmete jaoks nagu nutitelefonid, sülearvutid ja tahvelarvutid. Lisaks kasutatakse neid ka varutoiteallikana katkestusteta toitesüsteemides, et tagada kriitiliste süsteemide töövõime elektrikatkestuste ajal. Tänapäeval on oluline ülesanne vähendada süsinikdioksiidi heitkoguseid, mistõttu on akud olulised üleminekul kliimaneutraalsele majandusele, tootes säästvamaid elektrisõidukeid, aga ka toetades taastuvenergiaallikate arendamisel energiasalvestussüsteemidena.

Liitiumioonakud on üks populaarsemaid akutüüpe tänu nende suurele energiatihedusele, mis võimaldab salvestada palju energiat suhteliselt väikeses ja kerges kestas. See muudab liitiumioonakud sobivaks kasutamiseks kaasaskantavates elektroonikaseadmetes ja elektrisõidukites, kus kaal ja ruumipiirangud on olulised tegurid. Lisaks on liitiumioonakudel pikem tsükli kestus, suurem tõhusus ja kiirem laadimisaeg, mis teeb neist atraktiivse tööstusharu.

Kõige levinumad liitiumioonakud on valmistatud grafiitanoodist, kuid nende piiratud mahutavus ja kehv kestvus on teadlaste jaoks endiselt väljakutseid pakkuv teema, eriti elektrisõidukite rakenduste puhul. Teadlased on uurinud mitmeid uusi lahendusi, mis võivad oluliselt parandada akude jõudlust ja vähendada nende maksumust, muutes aku praktilisemaks ja taskukohasemaks laiemate rakenduste jaoks. SnO_2 nanoosakesed on teadlaste seas populaarsed materjalid, kuna neil on mitmeid olulisi omadusi. SnO_2 on pooljuht, mille keelutsoon on 3,6 eV, mistõttu neil on hea neeldumisvõime ja nad võivad paremini töötada koos grafiitanoodiga kui teised materjalid. Lisaks sellele on SnO_2 ökoloogiliselt puhas, odav ja rikkalikult saadaval, mis muudab selle väga atraktiivseks võimaluseks akuarenduseks. SnO_2 nanoosakesed võivad suurendada aku energiamahutavust ja pikendada aku eluiga, kuna need takistavad tahke elektrolüüdi liidese kasvu anoodi pinnal. Seetõttu võib SnO_2 kasutamine olla oluline samm tulevikus säästvamate ja tõhusamate energiasalvestustehnoloogiate väljatöötamisel.

Töö on jaotatud kaheks osaks. Esimene pool sisaldab kirjanduse ülevaadet patareidest ja tüüpidest, liitiumioonakudest ja nende tööprintsiibist, mis sisaldab täpsemat kirjeldust laadimis- ja tühjenemisprotsessist. Lisaks on välja toodud ülevaade nanomaterjalidest ja nende kasutusvõimalustest liitiumioonakudes. Eraldi peatükina on kirjeldatud erinevate materjalide (juht, pooljuht, isolaator) elektroonilised omadused, sh. tsooniteooriat, mis on oluline osa arusaamiseks SnO_2 nanomaterjalide uurimiseks. Antud peatükis selgitatakse täpsemalt erinevaid pooljuht materjale ja pooljuhtides esinevaid keelutsoone (keelutsoon ingl *bandgap* st energia kogus elektroni tõukamiseks valentstsoonilt juhtivustsooni, mõõdetakse elektronvoltides, eV-des), milleks on otsene keelutsoon (ingl *direct bandgap*) , kus materjalidel on suur neeldusmisvõime, kuna ei vaja palju energiat tõukeks. Kaudse keelutsooni (ingl *indirect bandgap*) materjalid, aga vajavad rohkem energiat, kuna tsoonide vahemik on paigast ära – vektoriaalselt puudub korrapärasus. Viimane osas antud peatükis annab ülevaate SnO_2 nanomaterjalist ja tema elektrokeemilistest omadustest. Töö teine osa sisaldab kasutatud uurimisseadmete, materjalide kirjeldust ja uurimismetoodikat. Tuuakse välja tehtud Tauc graafikute arvutusmeetodid, katsete läbiviimise kord ning tulemused ja analüüs. Antud töös on kasutatud Mendeley viitamissüsteemi.

Käesoleva lõputöö peamine eesmärk oli kasutada UV-Vis spektroskoopia analüüse, et uurida viie erineva SnO_2 nanomaterjali proovi elektroonilisi omadusi ja määrata nende keelutsooni energiavahemik. Konkreetne eesmärk oli uurida, kuidas temperatuur ja sünteesiaeg mõjutavad SnO_2 otsest ja kaudset keelutsooni, kasutades selleks Tauc graafiku arvutusi, kus tulemused uuriti kasutades Origin programmi. Kokkuvõtteks leiti, et otsene keelutsoon ei muutu temperatuuri ega sünteesi kestuse muutumisel, kuid täheldati, et mõlemad tegurid mõjutavad kaudset keelutsooni.

Antud töös leiti, et sünteesiaja kestus mõjutab kaudset keelutsooni, mille väärtused on vahemikus 3,65 eV kuni 3,80 eV. Sünteesiaja suurendamine 15 tunnilt 20 tunnile mõjutab kaudset keelutsooni, vähendades seda 3,80 eV-lt 3,65 eV-le. Sünteesi kestus ei avaldanud märkimisväärset mõju neeldumisspektrile, sest kõik proovid näitasid sarnast piiki väärtust vahemikus 276-280 nm, sõltumata sünteesi kestusest. Uurides SnO_2 defektiseisundeid, siis kergeid erinevusi võib täheldada nähtavas neeldumisspektris sünteesiaja suurenedes, mis tähendab, et pikema sünteesiajaga tekib materjalis rohkem defektitasandeid. Näiteks 20 tundi sünteesitud SnO_2 proovil ilmneb silmatorkavamalt rohkem defektiseisund võrreldes 6

tundi samades tingimustes sünteesitud prooviga. Kuna katse käigus SnO_2 pulbrit eelnevalt ei kaalutud, ei saa neeldumise intensiivsuse väärtusi võrrelda.

Teiseks uuriti, millist mõju avaldab SnO_2 nanoosakestele sünteesitemperatuuri muutus. Temperatuuri tõstmine 190 °C-lt 250 °C-le näitas viimase proovi puhul kõrgemat keelutsooni 4,16 eV, võrreldes 4,12 eV-ga, mis oli esimese proovi tulemus. Kuid erinevalt sünteesi kestusest ei tuvastatud erinevatel temperatuuridel sünteesitud proovide neeldumisspektrites olulist erinevust piikides, kuna kõik piikid näitasid sarnaseid väärtusi. Lisaks sellele viitab SnO_2 proovide otsene keelutsoon sellele, et sünteesi kestuse ja temperatuuri varieerumine mõjutab seda väheoluliselt, kusjuures otsese keelutsooni väärtused jäävad vahemikku 4,12 eV kuni 4,19 eV.

Käesolevas töös keskenduti sünteesitud SnO_2 nanomaterjalide elektrooniliste omaduste uurimisele ning seetõttu jääb defektide mõju elektrokeemilisele toimivusele vaatluse alt välja. Põhinedes nähtava valguse esinevate defektide analüüsil, saame valida SnO_2 nanomaterjali proovi, mis on kõige vähim esinevate defektseisundite arvuga (T190-06) ning sobib edasiseks põhjalikuks uurimiseks. Siiski on sünteesitud SnO_2 nanomaterjalide sügavama mõistmise saavutamiseks vajalik täiendavate analüüside läbiviimine, mis aitavad avastada materjali täpsemaid omadusi ja seeläbi suurendada arusaama selle potentsiaalsest kasutusvõimalustest erinevates akurakendustes.

APPENDIXES

LIHTLITSENTS

Lisa 1. Lihtlitsents lõputöö salvestamiseks ja üldsusele kättesaadavaks tegemiseks ning juhendajate kinnitus lõputöö kaitsmisele lubamise kohta

Mina, Julija Helm-Katšalov

sünniaeg 26.07.1986,

1. annan Eesti Maaülikoolile tasuta loa (lihtlitsentsi) enda koostatud lõputöö

"*SnO_2 Nanomaterials for Lithium-Ion Battery Applications* "
SnO_2 nanomaterjalide kasutus liitiumioonakudes

mille juhendajad on Protima Rauwel, Erwan Yann Rauwel, Reynald Songphon Ponte

1.1. salvestamiseks säilitamise eesmärgil,
1.2. digiarhiivi DSpace lisamiseks ja
1.3. veebikeskkonnas üldsusele kättesaadavaks tegemiseks

kuni autoriõiguse kehtivuse tähtaja lõppemiseni;

2. olen teadlik, et punktis 1 nimetatud õigused jäävad alles ka autorile;
3. kinnitan, et lihtlitsentsi andmisega ei rikuta teiste isikute intellektuaalomandi ega isikuandmete kaitse seadusest tulenevaid õigusi.

Lõputöö autor Julija Helm-Katšalov */ Allkirjastatud digitaalselt/*

Tartu, 03.06.2023
(*kuupäev*)

Juhendaja(te) kinnitus lõputöö kaitsmisele lubamise kohta

Luban lõputöö kaitsmisele.

Prof. Protima Rauwel, *PhD*
/Allkirjastatud digitaalselt/ Kuupäev

Prof. Erwan Yann Rauwel, *PhD, DSc*
/Allkirjastatud digitaalselt/ Kuupäev

Mr. Reynald Songphon Ponte, *MSc*
/Allkirjastatud digitaalselt/ Kuupäev